# Specificity of the Synergistic Anion for Iron Binding by Ferric Binding Protein from *Neisseria gonorrhoeae*†

Elena G. Bekker,‡ A. Louise Creagh,§ Nooshafarin Sanaie,§ Fumiaki Yumoto,# Gloria H. Y. Lau,|| Masaru Tanokura,# Charles A. Haynes,§ and Michael E. P. Murphy*,‡

*Department of Microbiology and Immunology, University of British Columbia, 6174 University Boulevard, Vancouver, BC V6T 1Z3, Canada, Biotechnology Laboratory and Department of Chemical and Biological Engineering, University of British Columbia, Vancouver, BC V6T 1Z3, Canada, Department of Applied Biological Chemistry, University of Tokyo, 1-1-1 Yayoi, Bunkyo-ku, Tokyo 113-8657, Japan, and Department of Biochemistry and Molecular Biology, University of British Columbia, 2146 Health Sciences Mall, Vancouver, BC V6T 1Z3, Canada*

*Received November 28, 2003; Revised Manuscript Received April 8, 2004*

ABSTRACT: Ferric binding protein in *Neisseria gonorrhoeae* (nFbpA) transports iron from outer membrane receptors for host proteins across the periplasm to a permease in an alternative pathway to the use of siderophores in some pathogenic bacteria. Phosphate and nitrilotriacetate, both at pH 8, and vanadate at pH 9 are shown to be synergistic in promoting ferric binding to nFbpA, in contrast to carbonate and sulfate. Interestingly, only phosphate produces the fully closed conformation of nFbpA as defined by native electrophoresis. The role of phosphate was probed by constructing three mutants: Q58E, Q58R, and G140H. The anion and iron binding properties of the Q58E mutant are similar to the wild-type protein, implying that one phosphate oxygen is a hydrogen bond donor and may in part define the specificity of nFbpA for phosphate over sulfate. Phosphate is a weakly synergistic anion in the Q58R and G140H mutants, and these mutants do not form completely closed structures. Ferric binding was investigated by both isothermal titration and differential scanning calorimetry. The apparent affinity of nFbpA for iron in a solution of 30 mM citrate is 1 order of magnitude larger in the presence ($K_{app} = 1.7 \times 10^5$ $M^{-1}$) of phosphate than in its absence ($K_{app} = 1.6 \times 10^4$ $M^{-1}$) at pH 7. Similar results were obtained at pH 8. This increase in affinity with phosphate as well as the formation of closed structure allows nFbpA to compete for free ferric ions in solution and suggests that ferric binding to nFbpA is regulated by the synergistic phosphate anion at sites of iron uptake.

Iron is a scarce but essential nutrient for most pathogens, and acquisition of iron from the host is a requirement for growth (*1*). As a result, host organisms have developed iron transport systems using proteins such as transferrin and lactoferrin that sequester iron tightly in an attempt to make iron unavailable to microbial pathogens. In response, pathogens have evolved complex systems to acquire iron from the host environment (for a review, see refs *2* and *3*). The well-known bacterial systems involve the elaborate synthesis of siderophores, small molecules that compete for iron with host proteins by chelating iron more tightly prior to binding to siderophore receptors on the bacterial cell surface. Another mechanism for iron sequestration is found in pathogens such as *Neisseria* and *Haemophilus* species that produce receptors for host iron containing molecules such as transferrin and lactoferrin (*4*−*6*). Ferric binding protein (FbpA)[1] is a soluble protein expressed under iron limiting conditions and localized to the periplasm (*7*). FbpA receives ferric ion ($Fe^{3+}$) from bacterial receptors for host iron proteins located on the outer membrane for transport to an iron permease at the inner membrane (*8*). The increase in virulence of *Neisseria* cultured under limiting iron (*9*) and the central link FbpA plays in the movement of iron from external receptors to the cell indicate that this protein is a promising therapeutic target.

FbpA is conserved among pathogenic *Neisseria* species (*10*), and homologues have been identified in other pathogenic bacteria such as *Haemophilus influenzae, Serratia marcescens*, and *Yersinia enterocolitica* (*11*, *12*). nFbpA purified from *Neisseria gonorrhoeae* is a 34-kDa basic protein (pI > 9.35) that binds one ferric ion (*13*−*15*). The crystal structure of HitA, the nFbpA homologue from *H. influenzae* (71% amino acid sequence identity), revealed that the protein comprises two domains with folds typical of the

† This work was supported by a Canadian Institutes of Health Research (CIHR) grant MT-14767 and MOP-49597 to M.E.P.M. who is also a CIHR scholar. G.H.Y.L. was supported by a National Science and Engineering Research Council (NSERC) studentship.

* Corresponding author. Phone: 604-822-8022; fax: 604-822-6041; e-mail: memurphy@interchange.ubc.ca.

‡ Department of Microbiology and Immunology, University of British Columbia.

§ Biotechnology Laboratory and Department of Chemical and Biological Engineering, University of British Columbia.

# University of Tokyo.

|| Department of Biochemistry and Molecular Biology, University of British Columbia.

[1] Abbreviations: FbpA, general name for ferric binding proteins; nFbpA, ferric binding protein from *Neisseria gonorrhoeae*; HitA, ferric binding protein from *Haemophilus influenzae*; hTf, human transferrin; NTA, nitrilotriacetate; MES, 2-[*N*-morpholino]ethanesulfonic acid; EDTA, ethylenediaminetetraacetic acid; OTf, ovotransferrin; hTf, human transferrin; DSC, differential scanning calorimetry; ITC, isothermal titration calorimetry.

10.1021/bi036143q CCC: $27.50 
Published on Web 06/19/2004

periplasmic $Fe^{3+}$-binding protein family and transferrin (*16*). The iron is bound at the interface between these two domains and is ligated by a phosphate anion, a water molecule, and a complement of protein residues: His9, Glu57, Tyr195, and Tyr196, all of which are conserved in the nFbpA. A similar lower resolution crystal structure of nFbpA (entry 1D9Y) is deposited in the Protein Data Bank.

nFbpA shares several physical and functional properties with transferrin. Both proteins possess similar protein ligands to iron (*16*), reversibly binding iron with high affinity, and display visible absorbance maxima in the 460−480 nm range (*13*). nFbpA and the individual lobes of transferrin exist in two distinct conformations depending on whether metal is bound (*17*, *18*). The most notable feature of nFbpA is the participation of a phosphate anion as a monodentate ligand to the ferric ion (*16*). The analogous synergistic carbonate anion in transferrin at neutral pH is a bidentate ligand to the iron; however, at pH 6 the carbonate becomes monodentate likely due to protonation (*19*). Iron release from transferrin occurs in acidified vesicles after cellular internalization. In contrast, nFbpA release of iron within the periplasm is not likely to be pH dependent and occurs by some alternative mechanism. Iron reduction has been suggested (*20*), although no reductase has been identified.

The objective of this study is to define experimentally the functional role of phosphate in ferric binding to nFbpA. The phosphate binding site in nFbpA involves direct interaction with seven residues: Glu57, Gln58, Ser139, Gly140, Ala141, Asn175, and Asn193, two of which were selected for mutagenesis to assess the role of phosphate in ferric binding. The mutant G140H was designed to provide an additional hydrogen bond to bound phosphate. The variant Q58E is observed in nFbpA homologues, and the Q58R mutation was designed to completely displace phosphate. The binding of synergistic anions and iron was assessed using UV−visible spectroscopy and both isothermal titration (ITC) and differential scanning (DSC) calorimetry.

## EXPERIMENTAL PROCEDURES

*Materials.* To remove trace metal contamination, all glassware was soaked in 6 M HCl and rinsed with deionized water (passed through a Millipore Milli-Q system). All chemical reagents were of analytical grade. Tris and sodium phosphate (dibasic) were purchased from Fisher Scientific, and all other reagents came from Sigma. Stock solutions of sodium phosphate, disodium salt of nitrilotriacetic acid (NTA), sodium bicarbonate, sodium sulfate, sodium citrate (1 M), and sodium orthovanadate (0.1 M) were prepared by dissolving the salts in Milli-Q water and adjusting the pH to 8 with 1 N NaOH or HCl. A solution of ferric chloride (10 mM) was prepared fresh every day and stored at 4 °C during the working day. To make a 3.5 mM solution of $FeCl_3$ in 30 mM citrate, 10 mM Tris buffer, pH 7 or 8, ferric chloride was first dissolved in the buffer and then the pH was adjusted with 1 N KOH. Solutions of 3.5 mM of ferric chloride containing 0.1 M phosphate were prepared by dissolving ferric chloride and sodium phosphate (monobasic and dibasic forms) in 30 mM citrate, 10 mM Tris buffer and then adjusting the pH with 1 N KOH. Ultrafiltration membranes (YM 10) were from Amicon.

*Cloning and Protein Expression.* For mutagenesis, the *fbpA* gene (*21*) was subcloned into Bluescript II $SK^-$. This construct was used to prepare the G140H, Q58E, and Q58R mutants as described by Nelson and Long (*22*) using the following primers to introduce the desired mutations: G140H, 5′-CAAGAACGCGTGGGAAGT-3′; Q58E, 5′-GGGATTTC-TTCGGAATAGAATAC-3′; Q58R, 5′-GGGATTCGTTCG-GAATAGA ATAC-3′. In each primer, the mutated codon is underlined. The complete nucleotide sequence of each mutant was determined to confirm the introduction of the specific mutations prior to recombinant expression in *Escherichia coli* by transformation with the relevant gene clone into the pTrc99a vector (Amersham). The recombinant proteins were purified as described previously with minor modifications (*13*). Purification was initiated by cell lysis with cetyltrimethylammonium bromide followed by one-step chromatography on CM-Sepharose CL-6B (Amersham). Holo-proteins were eluted from a column of CM-Sepharose with 300 mM NaCl in 25 mM Tris buffer, pH 8. To obtain the apo-form of the proteins, a CM-Sepharose column with protein adsorbed under initial conditions was washed with 10 mM citrate, 10 mM Tris buffer, pH 8 (3 column volumes), and then the protein was eluted from the column with 30 mM citrate, 10 mM Tris, pH 8. Apo- and holo-proteins were concentrated using YM10 Amicon ultrafiltration membrane and stored at −70 °C in 30 mM citrate, 10 mM Tris buffer, pH 8 and 300 mM NaCl, 25 mM Tris buffer, pH 8, respectively. For protein quantification, an extinction coefficient of 1.0 $(mg/mL)^{-1}$ $cm^{-1}$ at 280 nm was used based on both the Lowry (*23*) and Bradford (*24*) methods. Samples of wild-type nFbpA and mutants were analyzed by mass spectrometry, and the expected mass was observed for each sample (Table 1).

Table 1: Properties of Native and Mutant Forms of nFbpA

| nFbpA | mass (Da) | $\lambda_{max}$[a] (nm) |
|---|---|---|
| wild-type | 33,648 (33,639)[b] | 480 |
| Q58E | 2 (1) | 475 |
| G140H | 79 (80) | 460 |
| Q58R | 26 (27) | 430 |

[a] Maximal wavelength for holo-proteins obtained from spectra of Figure 1. [b] The absolute mass of the wild-type nFbpA is given along with the theoretical mass in parentheses. The values for the mutants are the observed and theoretical mass (in parentheses) differences relative to the wild-type.

*Iron Release and Binding*. For deferration of holo-protein with citrate as a chelator, a solution of nFbpA diluted to 3 mg/mL (0.089 mM) in 200 mM NaCl, 10 mM Tris, pH 8 (buffer A), was exposed to a 1300-fold molar excess (0.12 M) of sodium citrate for 10 min. Sodium citrate was removed from the deferrated protein by gel filtration on a Bio-Gel P-6 column (Biorad Ltd.) equilibrated with buffer A.

Solutions of apo-proteins (2.6 mg/mL) in buffer A were adjusted to 0.075 mM $FeCl_3$ at room temperature. Visible spectra were measured for 10 min before a 700-fold molar excess of the corresponding salt, pH 8, was added. The salts $Na_2HPO_4$, $NaHCO_3$, $Na_2C_6H_7NO_6$ ($Na_2$-NTA), $Na_2SO_4$, $Na_2C_4H_4O_4$ ($Na_2$-succinate), $NaCH_3COO$, $Na_2C_{10}H_{14}N_2O_8$ ($Na_2$-EDTA), $C_6H_8O_7Na_3$ ($Na_3$-citrate) were used as a source of phosphate, carbonate, nitrilotriacetate, sulfate, succinate, acetate, EDTA and citrate anions, respectively. After anion addition, visible spectra were taken every 2 min until the readings no longer changed (20 min). Vanadate anion, $VO_4^{3-}$, is stable in dilute and basic (pH 8−13) solutions (*25*);

at lower pH values, protonation and dehydration occur to form $(V_2O_7)^{4-}$ and higher vanadates. For this reason, all experiments with vanadate anion were performed at pH 9 and only with a 70-fold molar excess of anion over protein. The wavelength of maximum absorbance of the $Fe^{3+}$−protein−phosphate complex was selected to follow the changes in iron binding (Table 1). When NTA and vanadate binding were studied, the absorbance at 460 nm was used. Equimolar citrate anion was added because higher concentrations chelate iron from the protein.

All visible spectra and kinetic curves were obtained with a Cary50 Bio UV−visible spectrophotometer. Spectra of the proteins (3 mg/mL) in buffer A were recorded in the 350−700 nm range.

*Native Electrophoresis.* Native gels were made using a separating gel buffer of 0.2 M MES adjusted to pH 6.8 by 1 M KOH (8% polyacrylamide gel) and the stacking gel buffer of 0.06 M MES adjusted to pH 8 by 1 M KOH (4% PAAG). Protein samples were diluted with sample buffer consisting of 0.03 M MES buffer, pH 8 and 10% glycerol to 1.5 mg/mL before loading. Electrophoresis was carried out at 40 mA for 2 h in 0.02 M MES/0.036 M imidazole buffer, pH 6.8. Proteins were stained with Coomassie blue R. After destaining, gels were scanned using AlphaImager 1200 software.

*Calorimetry*. ITC of apo-nFbpA and apo-forms of the mutants were carried out on a MCS-ITC (MicroCal LLC, Northampton, MA). Data analysis was performed using software (Origin) supplied by MicroCal. All titrations were performed in 30 mM citrate, 10 mM Tris, pH 7 or 8; phosphate, when present, was 0.1 M. For each titration, 26 consecutive 10 $\mu$L aliquots of 3.5 mM ferric chloride in 30 mM citrate, 10 mM Tris buffer, pH 7 or 8 were injected into the sample cell (volume = 1.3528 mL) containing 130−177 $\mu$M protein in the same buffer, pH 7 or 8, respectively. The time between each injection varied from 5 to 20 min depending on the kinetics of the binding reactions. Control experiments were performed by injecting 10 $\mu$L aliquots of ferric chloride into protein-free buffer. These heats were subtracted from the heats generated in the titrations with protein. Each ITC experiment was performed 2−3 times, and the average binding parameters and associated error were calculated.

$K_{app}$ is the equilibrium constant for the overall binding reaction that occurs in the ITC cell and therefore includes Fe·ligand dissociation and ferric ion binding to nFbpA. We wish to determine the equilibrium constant, $K$, for the binding of free ferric ion to nFbpA according to the following reaction:

$$Fe^{3+} + nFbpAH_3 \overset{K}{\leftrightarrow} Fe{\cdot}nFbpA + 3H^+ \quad (1)$$

where $K = ([Fe{\cdot}nFbpA][H^+]^3/[Fe^{3+}][nFbpAH_3])$. In the Fe binding literature, an effective binding constant, $K'_{eff}$, is often reported instead of $K$. The binding constants $K$ and $K'_{eff}$ are related by (*26*)

$$K'_{eff} = \frac{[Fe{\cdot}nFbpA]}{[Fe^{3+}][nFbpAH_3]} = \frac{K}{[H^+]^3} \quad (2)$$

Knowledge of the reaction pH therefore allows one to calculate $K'_{eff}$ from a measured $K$ value. At each injection point during an ITC titration, [Fe·nFbpA] can be calculated from the ratio of the cumulative heat and the apparent enthalpy of binding, $\Delta H_{b,app}$. The total iron concentration, $[Fe]_{tot}$, after each injection is given by

$$[Fe]_{tot} = [Fe] + [Fe{\cdot}nFbpA] + \sum_{i=1}^{m} a_i Fe_a ligand_b H_c \quad (3a)$$

$$[Fe]_{tot} = [Fe] + [Fe{\cdot}nFbpA] + \sum_{i=1}^{m} a_i \beta_{abc,i} [Fe]^a [ligand]^b [H]^c \quad (3b)$$

where $\beta_{abc,i}$ is the formation constant for the $i$th $Fe_a$−$ligand_b$−$H_c$ complex, and [ligand], [Fe], and [H] are the free concentrations of ligand, iron, and proton ions, respectively. Negative values of $c$ indicate the number of hydroxyl ions. An equivalent total mass balance can be written for the ligand, and for the proton (hydroxyl). Solution of the set of mass balance equations for iron, nFbpA, ligand, and protons using formation constants obtained from the literature for the $Fe_a$−$ligand_b$−$H_c$ complexes gives the free ferric ion and nFbpA concentrations in the ITC cell at any time. These results then allow calculation of $K'_{eff}$ using eq 2.

DSC experiments were carried out on a Calorimetry Sciences Corp. MC-DSC (CSC, Provo, UT) in 0.1 M phosphate, 30 mM citrate, 10 mM Tris buffer, pH 7. Thermograms were obtained at different Fe/apo-nFbpA molar ratios from 0 (i.e., apo-nFbpA) to 4. Data analysis was performed using software provided with the calorimeter; fitting the thermograms to a two-state model with ligand dissociation (*27*, *28*) provided an estimate of the Fe−nFbpA binding constant.

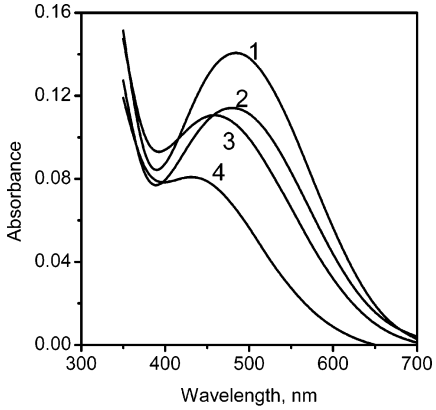


FIGURE 1: Visible spectra of wild-type nFbpA (1), Q58E (2), G140H (3), and Q58R (4) mutants (81 $\mu$M) in 200 mM NaCl, 10 mM Tris, pH 8.

## RESULTS

*Spectroscopic Characterization of Wild-Type and Mutant nFbpA.* Visible spectra of solutions (3 mg/mL) of purified recombinant wild-type and mutant nFbpA's have an absorption band in the 400−500 nm range (Figure 1, Table 1), indicating the formation of iron−phenolate bonds. Compared with pink colored wild-type nFbpA, the visible band of the Q58E mutant is slightly blue-shifted, whereas larger blue shifts of 20 and 50 nm are observed for the G140H and Q58R mutants, respectively. As a result, Q58R nFbpA is orange.

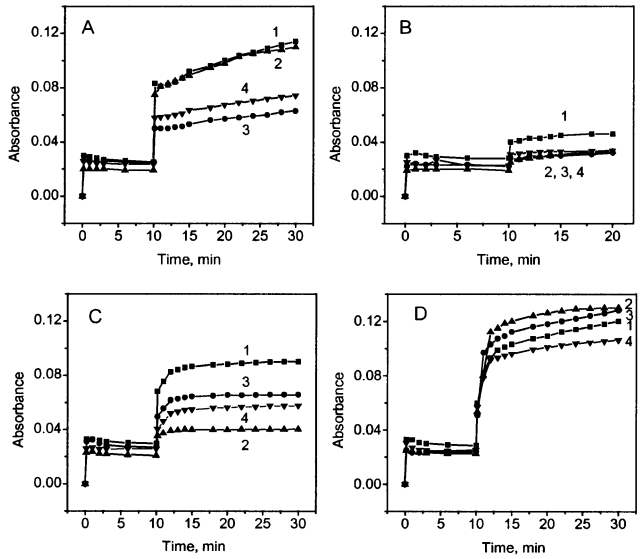


FIGURE 2: Anion dependence of iron binding. Apo-wild-type nFbpA (1), Q58E (2), G140H (3), and Q58R (4) mutants (75 $\mu$M) were incubated with ferric chloride (75 $\mu$M) for 10 min and then with phosphate (50 mM) (A), carbonate (50 mM) (B), vanadate (C) (5 mM), or nitrilotriacetate (D) (50 mM) for 20 min, in 200 mM NaCl, 10 mM Tris buffer, pH 8. (A, B) 480 nm (wild-type), 475 nm (Q58E), 460 nm (G140H), and 430 nm (Q58R), (C, D) 460 nm (all proteins). Absorbances of apo-proteins (A−D) and vanadate (C) were subtracted.

Ferric uptake by the apo-forms of wild-type and mutant nFbpA's was estimated by visible spectroscopy in the presence of a variety of potential synergistic anions. When equimolar ferric chloride was added to apo-nFbpA, weak ferric binding was detected by a small increase in visible absorbance (Figure 2). The addition of phosphate anions, the likely in vivo synergistic anion, produced a large increase in absorbance (Figure 2A), showing a role for phosphate in iron binding. The effect of carbonate anions on iron binding by the wild-type and mutant nFbpA's is much weaker than that of phosphate anions (Figure 2B). Notably, iron binding by wild-type nFbpA is promoted by vanadate anion (at pH 9) producing an absorbance peak at 460 nm. The synergistic effect of vanadate on the iron binding was less for the three mutant nFbpA's (Figure 2C). Nitrilotriacetic acid is a ferric ion chelator that is commonly used to provide soluble ferric ions to biological systems. Adding NTA anion to both wild-type and mutant nFbpA's resulted in a sharp increase in ferric binding (Figure 2D), suggesting that $NTA^{3-}$ serves as a nonphysiological synergistic anion for nFbpA. Interestingly, all Fe−nFbpA−NTA complexes have the same absorbance maximum (460 nm) independent of the wild-type or mutant form of nFbpA studied. Furthermore, the increase in absorption upon NTA addition is nearly the same for all nFbpA's tested. Sulfate anions did not promote ferric binding to either wild-type or mutant nFbpA's. Succinate, acetate, EDTA, and equimolar citrate were also not synergistic for ferric binding to wild-type nFbpA.

*Conformational States of apo- and holo-nFbpA's.* In the absence of ligand, the lobes of hTf are observed to have a more open structure (*29*). Similarly, periplasmic binding proteins have open and closed conformations in the absence and presence of ligand, respectively (*30*). The open and closed states of nFbpA were characterized previously by measuring trypsin sensitivity (*18*). A native gel electrophoresis method was developed to more directly assess the conformational state of wild-type and mutant nFbpA's. This method distinguishes clearly between the apo-, binary $Fe^{3+}$−nFbpA complex, and ternary $Fe^{3+}$−nFbpA−phosphate complex conformations. Apo-nFbpA has an open conformation and lower mobility on native gels relative to holo-nFbpA, which has a higher mobility and "closed conformation" (Figure 3A, lanes 1 and 3). The electrophoretic mobilities of native and mutant forms of nFbpA are similar due to the large net charge (+10) of native nFbpA. Apo-nFbpA plus $FeCl_3$ but without a synergistic anion displays two bands on these gels corresponding to the presence of both conformations in the sample (Figure 3A, lane 2). The observation of two bands is referred to as the half-closed conformation. When phosphate anion is added to the binary $Fe^{3+}$−nFbpA complex, the protein adopts the closed conformation characteristic of holo-nFbpA. Interestingly, the open conformation is obtained when NTA is added (Figure 3A, lane 4),

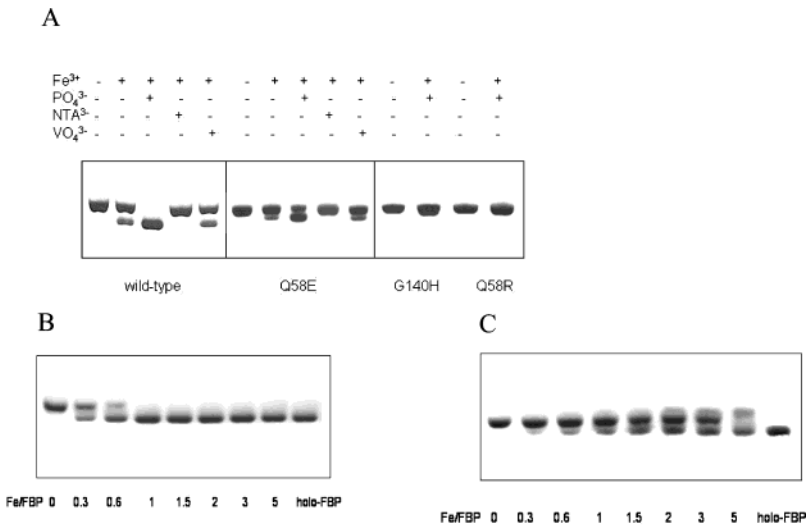


FIGURE 3: (A) Native electrophoresis of apo-proteins, complexes with $Fe^{3+}$, and complexes with $Fe^{3+}$ and different anions in 200 mM NaCl, 10 mM Tris buffer, pH 8. (B) Native electrophoresis of $Fe^{3+}$−nFbpA−phosphate complexes at different $Fe^{3+}$/nFbpA ratios in 0.1 M phosphate, 30 mM citrate, 10 mM Tris buffer, pH 7. (C) Native electrophoresis of $Fe^{3+}$−nFbpA complexes at different $Fe^{3+}$/nFbpA ratios in 30 mM citrate, 10 mM Tris buffer, pH 7.

whereas the addition of vanadate (at pH 9) did not alter the half-closed conformation of $Fe^{3+}$−nFbpA's as defined by this method (Figure 3A, lane 5). Migration of the Q58E mutant is similar to wild-type in the presence of the same anions except the closed conformation appears less compact (Figure 3A, lanes 6−10). In the case of the G140H and Q58R mutants, both the apo- and holo- forms are in the open conformation, as are the apo-forms reconstituted with iron and the panel of anions tested (Figure 3A, lanes 11−14, data with NTA and vanadate not shown). These results confirm that the mobility of nFbpA is not dependent on the net charge of the bound ligands but on the compactness of the resulting structure.

Native electrophoresis of the titration of apo-nFbpA with ferric chloride in the presence of phosphate and 30 mM citrate pH 7 is presented in Figure 3B. As expected, the change from the open to closed conformation is complete when the iron/apo-nFbpA ratio becomes 1:1 or higher. Native electrophoresis results of the nFbpA samples titrated with iron in the presence of phosphate at pH 8 are similar to the results at pH 7. The conformational state of the protein changes at different ratios of iron to apo-nFbpA even in the absence of phosphate (Figure 3C). As the iron-to-nFbpA ratio increased to three, the band corresponding to the closed conformation is detected. Above a ratio of five Fe/apo-nFbpA, a new band migrating slower than the apo-form appeared. Addition of excess ferric ions in the absence of phosphate has been shown to form a ferric hydroxide cluster at the iron binding site of nFbpA (*31*). This iron cluster may reduce the mobility of nFbpA in the gel by altering the protein conformation. Similar iron clusters are observed in mutant forms of HitA (*32*). Adjusting the pH to 8 resulted in similar conformational changes as observed by native electrophoresis.

*Calorimetry*. Figure 4A shows ITC data for the titration of apo-nFbpA with iron at pH 8 in the presence of phosphate (0.1 M). The integrated heats, after subtraction of the heat of dilution and normalized with the moles of iron injected, are shown in Figure 4B together with the binding-model fit. One iron binding site was observed on wild-type apo-nFbpA, with a $K_{app}$ of $4.6 \times 10^5$ $M^{-1}$ and a $\Delta H_{b,app}$ of 1.48 kcal/mol. At pH 8, in the absence of phosphate, the apparent binding constant and enthalpy of binding of iron to wild-type apo-nFbpA were $1.8 \times 10^4$ $M^{-1}$ and 0.51 kcal/mol, respectively. The ITC data for iron binding to the Q58E mutant at pH 8 in the presence of phosphate give a binding stoichiometry of about one, a $K_{app}$ of $1.0 \times 10^5$ $M^{-1}$, and a $\Delta H_{b,app}$ of 2.1 kcal/mol. For Q58R and G140H mutants, regressed $K_{app}$ values were lower, $2.1 \times 10^4$ and $8 \times 10^3$ $M^{-1}$, respectively.

At pH 7, in the absence of phosphate, an apparent binding constant and an enthalpy of binding of iron to wild-type apo-nFbpA were similar to those observed for the same system at pH 8, $K_{app}$ of $1.6 \times 10^4$ $M^{-1}$ and $\Delta H_{b,app}$ of 0.46 kcal/mol, respectively. Because of the complex nature of the ITC data at pH 7 in the presence of phosphate, it was not possible to use this technique to determine an apparent iron binding constant for nFbpA at this pH. An alternate method, DSC, was therefore used to estimate the apparent binding constant of iron to wild-type nFbpA at this pH.

Figure 4C presents denaturation thermograms for apo-nFbpA and holo-nFbpA in the presence of increasing iron

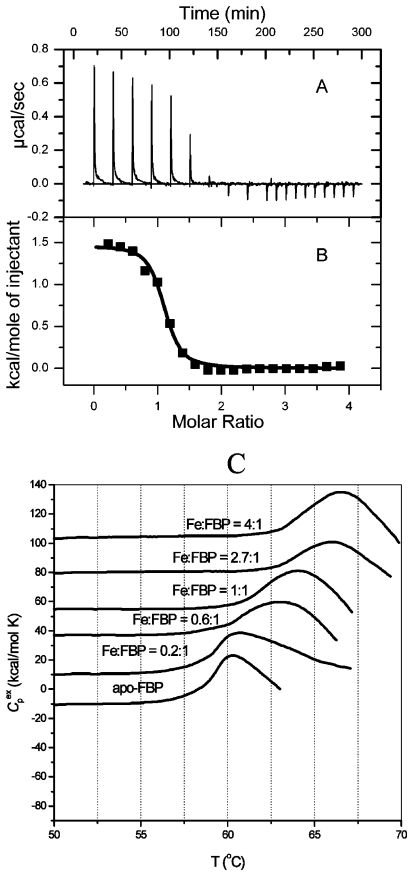


FIGURE 4: Raw data (A) and integrated heat changes fitted to one-site model (B) of ITC titration of 138 $\mu$M wild-type nFbpA with 3.5 mM $FeCl_3$ in 0.1 M phosphate, 30 mM citrate, 10 mM Tris buffer, pH 8. DSC scans (C) of nFbpA in 0.1 M phosphate, 30 mM citrate, 10 mM Tris pH 7 with different Fe−nFbpA ratios. Protein concentration varied in the samples from 0.12 to 0.16 mM, and the scan rate was 1 °C/min. For better understanding, DSC scans are arbitrarily shifted by the ordinate scale.

in 0.1 M phosphate, 30 mM citrate, 10 mM Tris buffer, pH 7. Unfolding of nFbpA is irreversible under these conditions; rescanning the samples results in little to no endotherm, and a white precipitate is found in the calorimetry cell following the experiment. Although unfolding is irreversible, Sánchez-Ruiz (*33*) has shown that the unfolding process can be modeled as reversible provided the shape and location of the unfolding thermogram (peak) are independent of scan rate. The thermogram shape and position were essentially identical for scan rates of 0.5 and 1 °C/min in our experiments, and the DSC data were therefore analyzed according to the two-state equilibrium model of Privalov (*34*) assuming no difference in the heat capacities of the native and denatured protein.

The DSC results support the binding of one iron per apo-nFbpA molecule. When the ratio of iron to nFbpA is greater than one, the shape of the thermograms does not change, and only a shift in the peak to a higher melting temperature $T_m$ is observed. In addition, the shape of the thermogram for nFbpA in the presence of equimolar amounts of iron and nFbpA is independent of the total concentration of iron and nFbpA up to a nFbpA concentration of 7 mg/mL. Binding thermodynamics for this system can therefore be determined from a global fit of the two-dimensional DSC model of Creagh et al. (*28*) to the DSC data by assuming that all transitions are two-state and the ligand binds only to the

native state of the protein. On the basis of this approach, $\Delta H_{N-U}(T_m)$, $K(T_m)$, $\Delta C_p(T_m)$, and $T_m$ (60.3 °C) data from DSC results for apo-nFbpA at pH 7 were used to regress a value for $K_b(T_m)$ of $1.8 \times 10^5$ $M^{-1}$. Using $\Delta H_{b,app}$ and $\Delta C_{pb}$ from ITC results then allows determination of an apparent binding constant for iron to nFbpA at 25 °C, $(1.7 \pm 0.4) \times 10^5$ $M^{-1}$. This value is similar to that determined by ITC for iron binding to nFbpA in the presence of phosphate at pH 8 and 25 °C.

## DISCUSSION

*Phosphate as a Synergistic Anion.* Of the physiological inorganic anions tested, phosphate is the strongly preferred synergistic anion for ferric binding to native and mutant nFbpA's (Figure 2). Carbonate anion was described as promoting ferric binding (*13*) and is able to replace phosphate in native nFbpA with prolonged incubation (*21*). The present assay demonstrates that nFbpA plus anion can directly compete for ferric ions with polymerization of ferric hydroxide. In this assay, carbonate is a much poorer synergistic anion than phosphate, suggesting that carbonate is not preferred for ferric ion uptake within the periplasm, where sufficient phosphate is available. Equimolar citrate also failed to enhance ferric binding to nFbpA by this assay. Vanadate ($VO_4^{3-}$) is able to substitute partially for phosphate in native nFbpA. On the basis of the similar extinction coefficients for hTf and nFbpA (*21*, *35*), we assume that molar absorptivity from bound iron does not depend on the nature or presence of the anion but is primarily determined by the number of coordinating tyrosines.

Interestingly, although sulfate is structurally similar to phosphate, little synergistic activity is observed. In the crystal structures of HitA and nFbpA, two of the three available phosphate oxygen atoms form hydrogen bonds with protein groups. Asn193, Asn175, and the main-chain amide of Gly140 are proton donors to one of these oxygens. The second oxygen of the phosphate appears to be a hydrogen bond donor to the O$\epsilon$1 atom of the Gln58 side-chain amide, indicating that the phosphate is bound in a protonated form. The fourth oxygen of phosphate bound to nFbpA does not interact with protein groups and is satisfied by water molecules instead. This free phosphate oxygen allows nFbpA to bind phosphate in both the mono- and dibasic forms. The structural determinants for specificity of phosphate over sulfate may be determined by the protonation state of the anion. At pH 8, sulfate ($SO_4^{2-}$) is unprotonated, whereas phosphate is protonated ($HPO_4^-$). Structural analysis and mutagenesis of a periplasmic binding protein that specifically recognizes phosphate but not sulfate reveal that Asp56 is the key determinant of specificity (*36*, *37*). The side-chain carboxylate of Asp56 acts as a hydrogen bond acceptor from bound dibasic phosphate. A requirement for a protonated phosphate for interaction with residue Gln58 of nFbpA would suggest that this residue plays a similar role in the specificity of phosphate over sulfate. Thus, as expected, the Q58E mutation does not greatly reduce phosphate synergism. Vanadate is also unprotonated at pH 9 but appears to be synergistic, likely due to a stronger interaction with ferric iron than sulfate. The Q58E mutation which introduces a negative charge into the anion binding site further weakens the interaction of vanadate with nFbpA, resulting in an observed loss of synergism (Figure 2C).

NTA, an organic nonphysiological ferric chelator, promotes ferric binding to nFbpA. NTA appears to be a universal synergistic anion, promoting ferric binding equally to mutant and native forms, suggesting that NTA binds independently of the nature of the phosphate binding site. NTA, pyrophosphate, and oxalate were found by UV−visible studies to be able to form $Fe^{3+}$−nFbpA−anion complexes (*21*, *38*). In hTf, a number of organic anions such as glyoxylate, glycolate, thioglycolate, glycine, oxalate, malonate bind weakly at the anion-binding site and substitute partially for bicarbonate (*29*, *39*). Recently, the crystal structure of the H9Q mutant of HitA revealed that EDTA may coordinate to the bound ferric ion; however, the overall structure is in an apo-like open conformation (*40*) analogous to the open structure for NTA observed by native electrophoresis.

*Ferric-Phosphate Cooperativity*. Phosphate binding is essential for forming the completely closed conformation of nFbpA (Figure 3A). Of all anions tested, none yield a nativelike closed conformation as observed in wild-type nFbpA, including NTA and vanadate, which are synergistic. Phosphate is poorly synergistic for iron binding to G140H and Q58R nFbpA, indicating that phosphate binding is important for iron binding. In addition, these mutants do not form the fully closed nFbpA conformation in the presence of phosphate (Figure 3A). These results suggest that the role of phosphate is not primarily to promote ferric binding but to stabilize the closed protein conformation to limit iron release. Interestingly, iron release is found to occur after protonation and dissociation of the phosphate from the protein (*41*). The native gel and calorimetry experiments are performed under equilibrium conditions, and kinetic data are needed to provide a complete description of the functional role of the phosphate.

Weakening of the phosphate nFbpA interaction strengthens the ferric tyrosine ligand interaction as shown by the blue shift in the visible absorption maxima. In general, the wavelength of maximum absorbance may indicate if ferric ions are bound in the closed conformation. Forms of nFbpA with a closed conformation (native and Q58E nFbpA with phosphate) show absorbance maxima at 480 nm, whereas for the open forms (native and mutant nFbpA's with NTA or vanadate, G140H and Q58R nFbpA with any anion) the maxima are shifted to the 430−460 nm region.

*Thermodynamics of Ferric Binding to nFbpA and Fe(III) Speciation.* While our initial spectroscopic studies confirm the role of the phosphate anion as the physiologically relevant synergistic ion, they do not quantify iron binding thermodynamics in the absence and presence of phosphate. Two modes of calorimetry were therefore used to further study nFbpA binding thermodynamics with the aim of establishing a more accurate comparison with the iron binding properties of human transferrin. All calorimetry experiments were performed in the presence of 30 mM citrate as a chelating ligand to keep iron soluble and as a competing agent to be able to measure the high binding affinity of nFbpA for iron. Our ITC results indicate that the apparent association constant, $K_{app}$, of iron to nFbpA in the presence of phosphate is 1 order of magnitude larger than in its absence.

In the absence of phosphate, citrate serves as the sole ligand for the ferric ion. On the basis of the set of iron−citrate complexes and associated formation constants reported

Table 2: Calculated Free Ferric Ion Concentration[a] and $K'_{eff}$ [a] for $Fe^{3+}$ Binding to nFbpA from ITC Data and Multiple-Chemical Equilibria[b]

| protein | $[Fe^{3+}]_{free}$ (M)[c] | $K'_{eff}$ ($M^{-1}$)[c] | $[Fe^{3+}]_{free}$ (M)[d] | $K'_{eff}$ ($M^{-1}$)[d] |
|---|---|---|---|---|
| | | In the Absence of Phosphate | | |
| wild-type | $4 \times 10^{-21}$ | $6 \times 10^{20}$ | $6 \times 10^{-27}$ | $4 \times 10^{26}$ |
| wild-type[e] | $(1.4 \pm 0.1) \times 10^{-19}$ | $(2 \pm 1) \times 10^{19}$ | $(7.3 \pm 0.7) \times 10^{-24}$ | $(3 \pm 2) \times 10^{23}$ |
| | | In the Presence of Phosphate | | |
| wild-type | $(2.7 \pm 0.2) \times 10^{-21}$ | $(7.2 \pm 0.4) \times 10^{21}$ | $(3.5 \pm 0.2) \times 10^{-27}$ | $(5.5 \pm 0.3) \times 10^{27}$ |
| Q58E | $(2.4 \pm 0.7) \times 10^{-21}$ | $(3 \pm 3) \times 10^{21}$ | $(3 \pm 1) \times 10^{-27}$ | $(2 \pm 2) \times 10^{27}$ |
| Q58R | $(4.5 \pm 0.1) \times 10^{-21}$ | $(6.0 \pm 0.1) \times 10^{20}$ | $(5.8 \pm 0.1) \times 10^{-27}$ | $(4.6 \pm 0.1) \times 10^{26}$ |
| G140H | $(3.2 \pm 0.2) \times 10^{-21}$ | $(6 \pm 2) \times 10^{20}$ | $(4.2 \pm 0.3) \times 10^{-27}$ | $(4 \pm 1) \times 10^{26}$ |

[a] Values reported are the averages of values calculated for data points in the center of the ITC titration, i.e., when the change in [Fe−nFbpA] is most significant. [b] All solutions are 30 mM citrate, 10 mM Tris and pH 8 except where indicated; all ITC experiments were performed at 25 °C. [c] Calculated using composite set of iron−citrate complexes suggested by Aisen et al. (*26*). [d] Calculated using iron−citrate complexes reported by Ribas et al. (*46*). [e] pH 7.

by Aisen et al. (*26*, *42*, *43*), our ITC data give a $K'_{eff}$ for wild-type nFbpA of ca. $2 \times 10^{19}$ $M^{-1}$ at pH 7 and $6 \times 10^{20}$ $M^{-1}$ at pH 8 (Table 2). Using the same set of iron−citrate complexes and formation constants, Dhungana et al. (*38*) report a $K'_{eff}$ of $1.4 \times 10^{17}$ $M^{-1}$ for ferric binding to nFbpA at pH 6.5 in the presence of citrate based on spectroscopic determination of [Fe−nFbpA]. Considering differences in pH, the results from the two independent methods are therefore fairly similar, indicating (particularly in the case of our results) that nFbpA binds iron with sufficient affinity to effectively eliminate any free iron (i.e., $[Fe^{3+}] \approx 0$) from the solution phase at total iron concentrations below the total concentration of nFbpA.

The value of $K'_{eff}$ derived from either ITC or spectroscopic data is, however, very sensitive to the set of iron−citrate complexes assumed present in the reaction mixture at the reaction pH. A number of iron−citrate species have been reported from potentiometric, polarographic, spectrophotometric, and magnetic susceptibility data (*42*−*47*). Regrettably, these studies, many of which were carried out prior to 1980, are highly conflicting; there is significant disagreement as to which ferric−citrate species (complexes) form, and, for a given species, there are usually differences in the reported formation constants. In addition, most of these studies were carried out under acidic conditions. In their studies of iron binding to transferrin, Aisen et al. (*26*) used a composite set of formation constants from the studies of Warner and Weber (*43*), in the pH range 1−5, augmented with data of Spiro et al. (*42*) taken in the pH range 7−10. However, Ribas et al. (*46*) have more recently used potentiometric titrations to provide a more comprehensive picture of iron−citrate speciation over the pH range 1.4−9.7. If the formation constants from this more complete analysis are used to calculate $K'_{eff}$ from ITC data, values 4−6 orders of magnitude higher than those calculated using the Aisen constants are obtained (Table 2).

The iron−citrate speciation data used by Aisen et al. (*26*) and the more comprehensive data of Ribas et al. (*46*) were also each used to calculate $K'_{eff}$ for iron binding to nFbpA in the presence of phosphate (Table 2). Using either the Aisen constants (*26*) or the Ribas constants (*46*), $K'_{eff}$ is 1 order of magnitude higher in the presence of phosphate than in its absence at pH 8 (Table 2). Dhungana et al. (*38*) also reported a 1 order of magnitude increase in $K'_{eff}$ when phosphate is present at pH 6.5.

Our ITC studies show that the mutant Q58E has similar binding characteristics to wild-type nFbpA. The other two mutants studied, Q58R and G140H, however, display significantly different binding thermodynamics for iron binding.

From DSC scans, the difference in $T_m$ between the apo- and holo-forms of wild-type nFbpA, 6.2 °C is not as large as observed for the C- or N-lobes of hTf (29 and 19 °C, respectively), which suggests a much lower apparent binding constant for Fe−citrate to nFbpA than for Fe−NTA to hTf. Indeed, the calculated apparent binding constant of iron to nFbpA by DSC is 8−16 orders of magnitude lower than that calculated from DSC data for hTf in the presence of Fe−NTA (1:2 molar ratio) and 25 mM bicarbonate at pH 7.5 ($1.1 \times 10^{22}$ $M^{-1}$ for the C-site and $8 \times 10^{13}$ $M^{-1}$ for the N-site) (*27*). Although the higher values for hTf may be overestimates because the $T_m$ values were controlled by kinetic factors at the scan rates used in the DSC experiments, nFbpA is unlikely to directly outcompete hTf for ferric ion, supporting a model for active transport of iron across the outer membrane.

*Comparison to Transferrin*. On the basis of the crystal structures of apo- and holo-HitA, Bruns et al. proposed that phosphate binds first to HitA preparing the protein for high affinity iron binding (*16*, *48*). In hTf, carbonate is a bidentate ligand that forms extensive hydrogen bond interactions with Arg124, Thr120 and backbone amides. The carbonate anion is proposed to bind first and neutralize the positive charge of Arg124 to prepare the site for metal binding by providing two potential ligands (*29*). In nFbpA, there are no positively charged groups near the active site and the anion provides only one ligand for the metal, and the active site in nFbpA is more solvent exposed than in transferrin (*48*). All these factors can explain why the affinity of wild-type nFbpA for iron in the absence of phosphate is only 10× weaker than in the presence of phosphate (apparent binding constants of $1.6 \times 10^4$ versus $1.7 \times 10^5$ $M^{-1}$ in 30 mM citrate, 10 mM Tris buffer pH 7). Furthermore, when excess iron is added to nFbpA in the presence of citrate but without phosphate, iron can bind and partly close the protein (Figure 3C). For hTf, the difference in apparent binding constants in the presence and absence of carbonate is much larger: 15 orders of magnitude for the C-lobe and 7 orders of magnitude for the N-lobe (*27*, *49*). By dialysis, the phosphate bound to holo-nFbpA may be replaced with other anions such as pyrophosphate, NTA, citrate, and carbonate (*38*). Interestingly, replacement of phosphate by these anions reduce the ferric binding constant by only 20× (*38*), suggesting that the nature of the anion is not critical for high-affinity iron binding.

However, phosphate appears to be essential for rapid iron uptake and formation of the closed conformation of the protein required for biological transport. The requirement of phosphate for ferric binding supports a model of nFbpA iron transport across the periplasm (*38*).

## ACKNOWLEDGMENT

The authors thank Dr. Ross MacGillivray for comments on the manuscript and many helpful discussions. We also thank Chris Petrus' assistance in preparing protein samples and Drs. Shouming He and Stephen Withers for mass spectrometry analysis of the proteins.

## REFERENCES

1. Cornelissen, C. N., and Sparling, P. F. (1994) Iron piracy: acquisition of transferrin-bound iron by bacterial pathogens, *Mol. Microbiol. 14*, 843−850.
2. Mietzner, T. A., Tencza, S. B., Adhikari, P., Vaughan, K. G., and Nowalk, A. J. (1998) Fe(III) periplasm-to-cytosol transporters of gram-negative pathogens, *Curr. Top. Microbiol. Immunol. 225*, 113−135.
3. Schryvers, A. B., and Stojiljkovic, I. (1999) Iron acquisition systems in the pathogenic *Neisseria*, *Mol. Microbiol. 32*, 1117−1123.
4. Archibald, F. S., and DeVoe, I. W. (1980) Iron acquisition by *Neisseria meningitidis* in vitro, *Infect. Immun. 27*, 322−334.
5. Mickelsen, P. A., and Sparling, P. F. (1981) Ability of *Neisseria gonorrhoeae*, *Neisseria meningitidis*, and commensal *Neisseria* species to obtain iron from transferrin and iron compounds, *Infect. Immun. 33*, 555−564.
6. Anderson, J. E., Hobbs, M. M., Biswas, G. D., and Sparling, P. F. (2003) Opposing selective forces for expression of the gonococcal lactoferrin receptor, *Mol. Microbiol. 48*, 1325−1337.
7. Mietzner, T. A., Luginbuhl, G. H., Sandstrom, E., and Morse, S. A. (1984) Identification of an iron-regulated 37,000-dalton protein in the cell envelope of *Neisseria gonorrhoeae*, *Infect. Immun. 45*, 410−416.
8. Adhikari, P., Berish, S. A., Nowalk, A. J., Veraldi, K. L., Morse, S. A., and Mietzner, T. A. (1996) The *fbpABC* locus of *Neisseria gonorrhoeae* functions in the periplasm-to-cytosol transport of iron, *J. Bacteriol. 178*, 2145−2149.
9. Keevil, C. W., Davies, D. B., Spillane, B. J., and Mahenthiralingam, E. (1989) Influence of iron-limited and replete continuous culture on the physiology and virulence of *Neisseria gonorrhoeae*, *J. Gen. Microbiol. 135*, 851−863.
10. Genco, C. A., Berish, S. A., Chen, C. Y., Morse, S., and Trees, D. L. (1994) Genetic diversity of the iron-binding protein (Fbp) gene of the pathogenic and commensal *Neisseria*, *FEMS Microbiol. Lett. 116*, 123−129.
11. Kirby, S. D., Lainson, F. A., Donachie, W., Okabe, A., Tokuda, M., Hatase, O., and Schryvers, A. B. (1998) The *Pasteurella haemolytica* 35 kDa iron-regulated protein is an FbpA homolog, *Microbiology 144*, 3425−3436.
12. Angerer, A., Gaisser, S., and Braun, V. (1990) Nucleotide sequences of the *sfuA*, *sfuB*, and *sfuC* genes of *Serratia marcescens* suggest a periplasmic-binding-protein-dependent iron transport mechanism, *J. Bacteriol. 172*, 572−578.
13. Nowalk, A. J., Tencza, S. B., and Mietzner, T. A. (1994) Coordination of iron by the ferric iron-binding protein of pathogenic *Neisseria* is homologous to the transferrins, *Biochemistry 33*, 12769−12775.
14. Chen, C. Y., Berish, S. A., Morse, S. A., and Mietzner, T. A. (1993) The ferric iron-binding protein of pathogenic *Neisseria* spp. functions as a periplasmic transport protein in iron acquisition from human transferrin, *Mol. Microbiol. 10*, 311−318.
15. Berish, S. A., Mietzner, T. A., Mayer, L. W., Genco, C. A., Holloway, B. P., and Morse, S. A. (1990) Molecular cloning and characterization of the structural gene for the major iron-regulated protein expressed by *Neisseria gonorrhoeae*, *J. Exp. Med. 171*, 1535−1546.
16. Bruns, C. M., Nowalk, A. J., Arvai, A. S., McTigue, M. A., Vaughan, K. G., Mietzner, T. A., and McRee, D. E. (1997) Structure of *Haemophilus influenzae* Fe(+3)-binding protein reveals convergent evolution within a superfamily, *Nat. Struct. Biol. 4*, 919−924.
17. Brock, J. H., Arzabe, F., Lampreave, F., and Pineiro, A. (1976) The effect of trypsin on bovine transferrin and lactoferrin, *Biochim. Biophys. Acta 446*, 214−225.
18. Nowalk, A. J., Vaughan, K. G., Day, B. W., Tencza, S. B., and Mietzner, T. A. (1997) Metal-dependent conformers of the periplasmic ferric ion binding protein, *Biochemistry 36*, 13054−13059.
19. MacGillivray, R. T., Moore, S. A., Chen, J., Anderson, B. F., Baker, H., Luo, Y., Bewley, M., Smith, C. A., Murphy, M. E., Wang, Y., Mason, A. B., Woodworth, R. C., Brayer, G. D., and Baker, E. N. (1998) Two High-Resolution Crystal Structures of the Recombinant N-Lobe of Human Transferrin Reveal a Structural Change Implicated in Iron Release, *Biochemistry 37*, 7919−7928.
20. Taboy, C. H., Vaughan, K. G., Mietzner, T. A., Aisen, P., and Crumbliss, A. L. (2001) $Fe^{3+}$ coordination and redox properties of a bacterial transferrin, *J. Biol. Chem. 276*, 2719−2724.
21. Guo, M., Harvey, I., Yang, W., Coghill, L., Campopiano, D. J., Parkinson, J. A., MacGillivray, R. T. A., Harris, W. R., and Saddler, P. J. (2003) Synergistic Anion and Metal Binding to the Ferric Ion-binding Protein from *Neisseria gonorrhoeae*, *J. Biol. Chem. 278*, 2490−2502.
22. Nelson, R. M., and Long, G. L. (1989) A general method of site-specific mutagenesis using a modification of the *Thermus aquaticus* polymerase chain reaction, *Anal. Biochem. 180*, 147−151.
23. Lowry, O. H., Rosbrough, N. J., Farr, A. L., and Randall, R. J. (1951) Protein measurement with the Folin phenol reagent, *J. Biol. Chem. 193*, 265−275.
24. Bradford, M. M. (1976) A rapid and sensitive method for the quantitation of microgram quantities of protein utilizing the principle of protein-dye binding, *Anal. Biochem. 72*, 248−254.
25. Pope, M. T. (1983) Inorganic Chains, Rings, Cages, and Clusters, in *Heteropoly and Isopoly Oxometalates*, p 756, Springer-Verlag, New York.
26. Aisen, P., Leibman, A., and Zweier, J. (1978) Stoichiometric and site characteristics of the binding of iron to human transferrin, *J. Biol. Chem. 253*, 1930−1937.
27. Lin, L.-N., Mason, A. B., Woodworth, R. C., and Brandts, J. F. (1994) Calorimetric studies of serum transferrin and ovotransferrin. Estimates of domain interactions, and study of the kinetic complexities of ferric ion binding, *Biochemistry 33*, 1881−1888.
28. Creagh, A. L., Koska, J., Johnson, P. E., Tomme, P., Joshi, M. D., McIntosh, L. P., Kilburn, D. G., and Haynes, C. A. (1998) Oligosaccharide Binding of the N1 Cellulose-Binding Domain of *Cellulomonas Fimi* Endoglucanase CenC, *Biochemistry 37*, 3529−3537.
29. Baker, E. N. (1994) Structure and reactivity of transferrins, *Adv. Inorg. Chem. 41*, 389−463.
30. Quiocho, F. A., and Ledvina, P. S. (1996) Atomic structure and specificity of bacterial periplasmic receptors for active transport and chemotaxis: variation of common themes, *Mol. Microbiol. 20*, 17−25.
31. Zhu, H., Alexeev, D., Hunter D. J. B., Campopiano, D. J., and Sadler, P. J. (2003) Oxo-iron clusters in a bacterial iron-trafficking protein: new roles for a conserved motif, *Biochem. J. 376*, 35−41.
32. Shouldice, S. R., Skene, R. J., Dougan, D. R., McRee, D. E., Tari, L. W., and Schryvers, A. B. (2003) Presence of Ferric Hydroxide Clusters in Mutants of *Haemophilus influenzae* Ferric Ion-Binding Protein A, *Biochemistry 42*, 11908−11914.
33. Sánchez-Ruiz, J. M. (1992) Theoretical analysis of Lumry-Eyring models in differential scanning calorimetry, *Biophys. J. 61*, 921−935.
34. Privalov, P. L. (1979) Stability of proteins. Small globular proteins, *Adv. Protein Chem. 33*, 167−241.
35. Gaber, B. P., Miskowski, V., and Spiro, T. G. (1974) Resonance Raman scattering from iron(III)- and copper(II)-transferrin and an iron(III) model compound. A spectroscopic interpretation of the transferrin binding site, *J. Am. Chem. Soc. 96*, 6868−6873.
36. Wang, Z., Choudhary, A., Ledvina, P., and Quiocho, F. (1994) Fine tuning the specificity of the periplasmic phosphate transport receptor. Site-directed mutagenesis, ligand binding, and crystallographic studies, *J. Biol. Chem. 269*, 25091−25094.
37. Luecke, H., and Quiocho, F. A. (1990) High specificity of a phosphate transport protein determined by hydrogen bonds, *Nature 347*, 402−406.

38. Dhungana, S., Taboy, C. H., Anderson, D. S., Vaughan, K. G., Aisen, P., Mietzner, T. A., and Crumbliss, A. L. (2003) The influence of the synergistic anion on iron chelation by ferric binding protein, a bacterial transferrin, *Proc. Natl. Acad. Sci. U.S.A. 100*, 3659−3664.
39. Schlabach, M. R., and Bates, G. W. (1975) The synergistic binding of anions and $Fe^{3+}$ by transferrin. Implications for the interlocking sites hypothesis, *J. Biol. Chem. 250*, 2182−2188.
40. Shouldice, S. R., Dougan, D. R., Skene, R. J., Tari, L. W., McRee, D. E., Yu, R.-h., and Schryvers, A. B. (2003) High-Resolution Structure of an Alternate Form of the Ferric Ion Binding Protein from *Haemophilus influenzae*, *J. Biol. Chem. 278*, 11513−11519.
41. Boukhalfa, H., Anderson, D. S., Mietzner, T. A., and Crumbliss, A. L. (2003) Kinetics and mechanism of iron release from the bacterial ferric binding protein nFbp: exogenous anion influence and comparison with mammalian transferrin, *J. Biol. Inorg. Chem. 8*, 881−892.
42. Spiro, T. G., Bates, G., and Saltman, P. (1967) Hydrolytic polymerization of ferric citrate. II. Influence of excess citrate, *J. Am. Chem. Soc. 89*, 5559−5562.
43. Warner, R. C., and Weber, I. (1953) The cupric and ferric citrate complexes, *J. Am. Chem. Soc. 75*, 5086−5094.
44. Konigsberger, L.-C., Konigsberger, E., May, P. M., and Hefter, G. T. (2000) Complexation of iron(III) and iron(II) by citrate. Implications for iron speciation in blood plasma, *J. Inorg. Biochem. 78*, 175−184.
45. Lanford, O. E., and Quinan, J. R. (1948) A spectrophotometric study of the reaction of ferric iron and citric acid, *J. Am. Chem. Soc. 70*, 2900−2903.
46. Ribas, X., Salvado, V., and Valiente, M. (1989) The chemistry of iron in biosystems. Part 2. A hydrolytic model of the complex formation between iron(III) and citric acid in aqueous solutions, *J. Chem. Res., Synop.* 332.
47. Yokoi, H., Mitani, T., Mori, Y., and Kawata, S. (1994) Complex formation between iron (III) and citric acids in a wide pH range 1 to 13 as studied by magnetic susceptibility measurements, *Chem. Lett.*, 281−284.
48. Bruns, C. M., Anderson, D. S., Vaughan, K. G., Williams, P. A., Nowalk, A. J., McRee, D. E., and Mietzner, T. A. (2001) Crystallographic and biochemical analyses of the metal-free *Haemophilus influenzae* $Fe^{3+}$-binding protein, *Biochemistry 40*, 15631−15637.
49. Lin, L.-N., Mason, A. B., Woodworth, R. C., and Brandts, J. F. (1993) Calorimetric studies of the binding of ferric ions to human serum transferrin, *Biochemistry 32*, 9398−9406.

BI036143Q